PHYSICAL REVIEW B **92**, 081306(R) (2015)

Large linear magnetoresistance in Dirac semimetal Cd_3As_2 with Fermi surfaces close to the Dirac points

Junya Feng, Yuan Pang, Desheng Wu, Zhijun Wang, Hongming Weng, Jianqi Li, Xi Dai, Zhong Fang, Youguo Shi,* and Li Lu†

Beijing National Laboratory for Condensed Matter Physics, Institute of Physics, Chinese Academy of Sciences, Collaborative Innovation Center of Quantum Matter, Beijing 100190, People's Republic of China

(Received 26 May 2014; revised manuscript received 30 July 2015; published 19 August 2015)

We investigated the magnetoresistive behavior of an ideal Dirac semimetal—high-quality single crystals of Cd_3As_2 with a Fermi level very close to the Dirac point. A large linear magnetoresistance (LMR), up to 3100% in a magnetic field of 14 T, was observed at a temperature of $T = 2$ K. The detailed field and temperature dependencies reveal that the LMR occurs only when the Zeeman energy surpasses the thermal energy. Our result hints that the field-induced relative shifting of the two Weyl-Fermi surfaces in each Dirac cone in momentum space is likely responsible for the LMR behavior.

DOI: 10.1103/PhysRevB.92.081306 PACS number(s): 75.47.−m, 71.70.Ej

Compared with those negative magnetoresistive behaviors, such as giant magnetoresistance [1] and colossal magnetoresistance [2], whose mechanisms have been well understood, positive linear magnetoresistance (LMR) was also extensively reported, but its mechanism has not yet been fully clarified. Positive LMR was previously found in highly disordered nonmagnetic narrow-band semiconductors, such as $Ag_{2\pm\delta}Te$ and $Ag_{2\pm\delta}Se$ [3], in bismuth thin films [4], in InSb [5], and recently in epitaxial graphene [6], topological insulators [7–9], and Dirac and Weyl semimetals [10–17].

A number of mechanisms have been proposed to explain the positive LMR behavior. Abrikosov proposed that it might arise from a linearly dispersed electron system when all the electrons are filled into the first Landau level (LL), i.e., in the extreme quantum limit [18,19]. Wang and Lei proposed that a LMR could still occur when multiple LLs are filled, even when thermal smearing is severe, as long as the system has a positive g factor [20]. There are also pictures involving no LLs. Parish and Littlewood explained the LMR in $Ag_{2\pm\delta}Te$ and $Ag_{2\pm\delta}Se$ by modeling the materials as a network due to disorder-induced mobility fluctuation [21]. So far the mechanism of LMR still needs to be clarified.

In this Rapid Communication, we revisit the LMR issue by investigating the magnetoresistive behavior of Cd_3As_2 single crystals. Cd_3As_2 was predicted to be a three-dimensional (3D) Dirac semimetal with linearly dispersed electron states in the bulk and Fermi arcs at the surface [22]. Experimentally, the existence of 3D Dirac cones has been confirmed by angular-resolved photoemission spectroscopy studies [23–25] and a scanning tunneling microscopy study [26]. A LMR behavior has recently been reported on this type of material with high carrier density (on the order of 10^{18} cm^{-3}) [10,11,13]. And the LMR behavior becomes more pronounced in multidomain samples [11].

Here, we report our magnetotransport study on high-quality single crystals of Cd_3As_2 with much lower carrier densities, a material which can be regarded as an ideal Dirac semimetal because their Fermi surfaces are small spheres very close to the Dirac points in the momentum space. We observed a very large LMR on this material, up to 3100% in a field of 14 T at $T = 2$ K. We found that the LMR occurs only when the Zeeman splitting energy surpasses the thermal energy. The implication of this result will be discussed.

Single crystals of Cd_3As_2 were synthesized via a two-step chemical vapor transport method whose details are presented in the Supplemental Material [27]. Two different phases of Cd_3As_2 were obtained, one with P_{42}/nmc symmetry [28] and the other with I_{41}/cd [29] or I_{41}/acd [30] symmetry. The platelike rectangular crystals studied in this experiment belong to the latter phase, whose crystal structure, x-ray diffraction pattern, and high-resolution transmission electron microscope (HRTEM) image are shown in Figs. 1(a)–1(c), respectively. All the peaks in Fig. 1(b) can be well indexed to the centered tetragonal structure of I_{41}/acd symmetry with lattice parameters $a = b = 12.6527$ Å and $c = 25.4578$ Å. A HRTEM study indicates that the platelike crystals grow preferentially along the [012] direction (the length direction) with the width direction along $[02\bar{1}]$ and the thickness direction along [100].

Hall-bar devices were defined by manually attaching six Pt wires of diameter 20 μm to each thin-plate crystal with the use of silver paste. The electric current was applied along the length direction, and the magnetic field was applied and rotating from the [100] to the $[02\bar{1}]$ directions as illustrated in the inset of Fig. 4(b). The longitudinal and Hall resistance measurements were carried out by using a standard lock-in technique in a physical property measurement system (Quantum Design) which has a base temperature of 2 K and a magnetic field up to 14 T.

About ten Hall-bar devices were studied, and reproducible results were obtainable. Presented here are the data obtained on one of the Hall-bar devices whose optical image is shown in the inset of Fig. 2(a). For this device, the width of the crystal is ∼150 μm, the distance between the voltage contacts is ∼450 μm, and the thickness of the crystal is ∼20 μm.

Shown in Fig. 2(a) is the resistivity of the crystal as a function of temperature. It has a semiconductorlike temperature dependence near room temperature and a metallic behavior below ∼100 K. We note that the high-temperature semiconducting behavior was only observable on crystals with very low carrier densities. This phenomenon was reproducible

*Corresponding author: ygshi@iphy.ac.cn
†Corresponding author: lilu@iphy.ac.cn

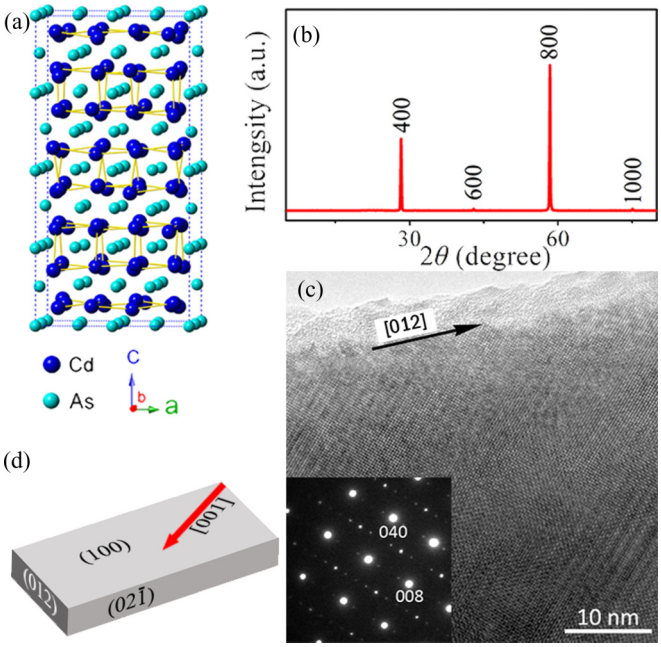

FIG. 1. (Color online) (a) Crystal structure of Cd_3As_2 with I_{41}/acd centrosymmetry viewed along the [010] direction (the b direction). (b) X-ray diffraction pattern of platelike rectangular Cd_3As_2 crystals used in this experiment. (c) High-resolution transmission electron microscope image and selected-area electron-diffraction pattern (inset) of a platelike Cd_3As_2 crystal taken along the [100] zone-axis direction, i.e., the electron-beam incidents perpendicular to the largest facet of the crystal. (d) The indexes of the facets of the platelike crystals. The arrow indicates the [001] zone-axis direction.

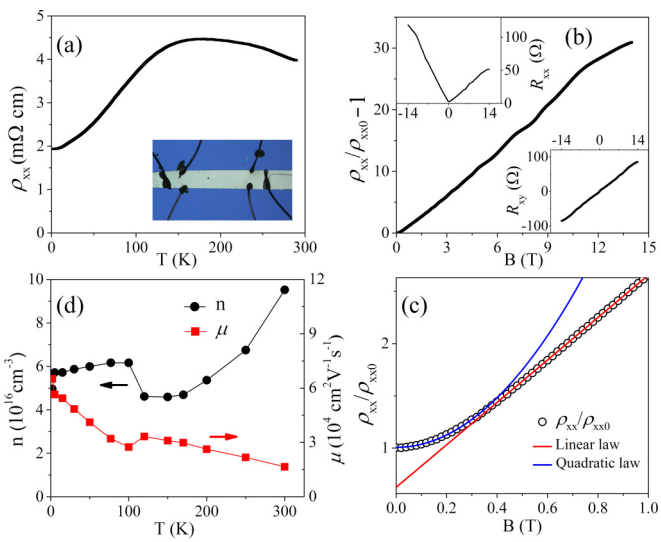

FIG. 2. (Color online) (a) The temperature dependence of longitudinal resistivity ρ_{xx} of Cd_3As_2. Inset: the optical image of the Hall-bar device defined on a thin plate of Cd_3As_2 crystal on which the data were measured. (b) Main frame: the magnetoresistivity $\rho_{xx}/\rho_{xx0}-1$ measured at 2 K (where ρ_{xx0} is the longitudinal resistivity in the zero magnetic field). These data have been symmetrized by averaging over the positive and negative field directions. Upper left inset: original (unsymmetrized) data of R_{xx}. Lower right inset: the Hall resistivity R_{xy} measured at 2 K. (c) Details of ρ_{xx}/ρ_{xx0} below $B=1$ T. (d) The temperature dependencies of the carrier density and the Hall mobility.

on crystals of different batches. The semiconducting behavior is presumably contributed by the thermally excited carriers due to the existence of, e.g., point defects in the crystal, similar to the case in InSb [5]. With decreasing temperature, the thermally excited carriers gradually freeze-out, leading to a less temperature-dependent carrier density [Fig. 2(d)] and thus a metallic temperature dependence of resistivity below ~100 K.

For samples with low carrier densities, their Hall resistivity could be larger than the longitudinal one ρ_{xx}, thus influencing the accurate measurement of the latter. Nevertheless, the Hall signal mixed into ρ_{xx} can be removed by averaging the raw data of ρ_{xx} over the positive and the negative field directions. From the raw ρ_{xx} data measured at 2 K [shown in the upper-left inset of Fig. 2(b)], we obtained the symmetrized (intrinsic) longitudinal resistance, which are plotted as $\rho_{xx}/\rho_{xx0}-1$ in the main frame of Fig. 2(b) (where ρ_{xx0} denotes the longitudinal resistance in the zero magnetic field). A very large LMR up to 3100% in a field of 14 T can be seen, accompanied with obvious Shubnikov–de Haas (SdH) oscillations.

Figure 2(c) further shows that the LMR behavior extends to a field as low as ~0.35 T where no sign of SdH oscillations can be resolved. Below ~0.35 T, however, a quadratic law restores.

From the Hall slope $R_H=-1/ne$ of the data shown in the lower-right inset of Fig. 2(b), the carrier density can be deduced: $n=5.0\times10^{16}$ cm^{-3}. According to the Drude conductivity $\sigma=ne\mu$, the effective electron mobility is then: $\mu=6.5\times10^4$ cm^2 V^{-1} s^{-1}. The temperature dependencies of n and μ are plotted in Fig. 2(d). It can be seen that n is almost constant below ~100 K, whereas μ changes by a factor of 2. The n estimated from the Hall measurement roughly agrees with that estimated from the SdH oscillation after ellipsoid correction, which is 2.5×10^{17} cm^{-3}, indicating that the measured signals come from a 3D electron system in Cd_3As_2. The estimation of the carrier density from the SdH oscillations, together with the estimations of the effective electron mass $m^*=0.025m_e$ and the Dingle temperature $T_D=12$ K, can be found in the Supplemental Material [27].

Shown in Fig. 3(a) is the field dependence of ρ_{xx} measured at different temperatures. ρ_{xx} changes from a quadratic field dependence near room temperatures to a linear field dependence below 100 K. This evolution can be more clearly seen from the first-order derivative of the data shown in Fig. 3(b). The $d\rho_{xx}/dB$ starts with a linear behavior from $B=0$, indicating that a quadratic magnetoresistive behavior dominates in the low-field regime (regime I). With increasing the magnetic field to above a crossover field B_c, $d\rho_{xx}/dB$ enters into regime II. In this regime $d\rho_{xx}/dB$ eventually becomes flat at low temperatures, demonstrating a dominant LMR behavior.

The temperature dependencies of the intercept and the slope of $d\rho_{xx}/dB$ in regime II are plotted in Fig. 3(c). It can be seen that the intercept (corresponding to the amplitude of the LMR) is the biggest and almost temperature independent below ~100 K. It decreases with increasing temperature above ~100 K and finally vanishes around room temperature. The slope plotted in Fig. 3(c) corresponds to the amplitude of the quadratic component. It gradually increases with temperature, but its contribution to the total magnetoresistance is small and hardly recognizable except when the intercept drops to zero near room temperature.

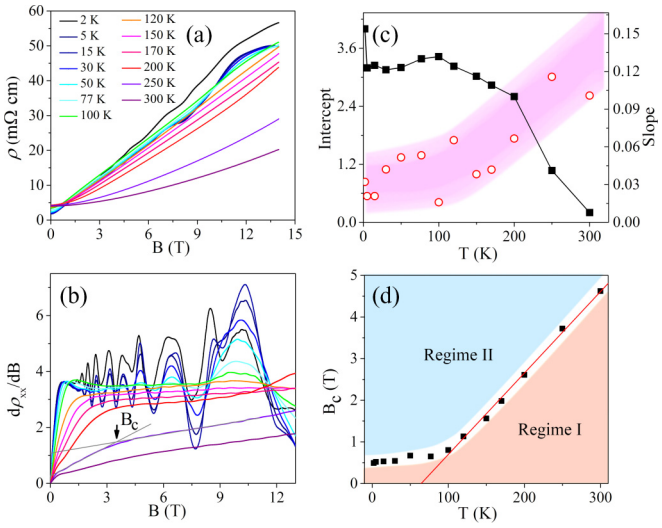

FIG. 3. (Color online) (a) The field dependence of ρ_{xx} measured at different temperatures. (b) The $d\rho_{xx}/dB$ at different temperatures. The arrow indicates the crossover field B_c between regime I and regime II (see the context). (c) The temperature dependencies of the intercept (black squares) and the slope (red circles) of $d\rho_{xx}/dB$ in regime II. (d) The temperature dependence of the crossover field B_c.

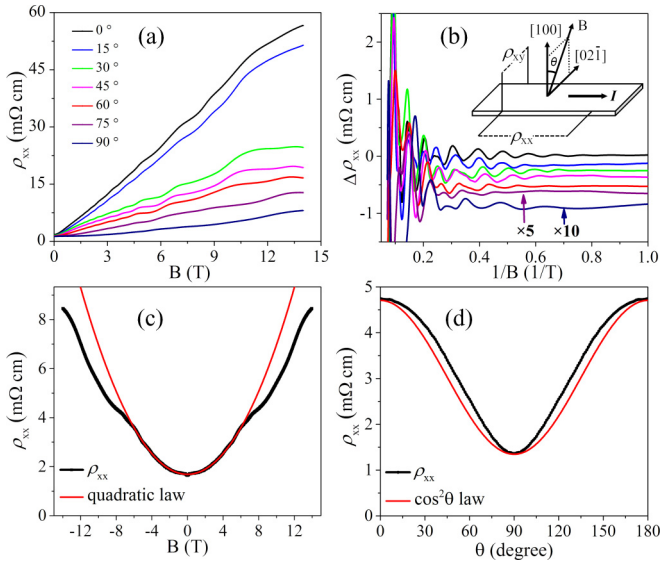

FIG. 4. (Color online) (a) ρ_{xx} measured at $T = 2$ K and in tilted magnetic fields with the measurement configuration illustrated in the inset of (b). (b) The data in (a) are replotted against $1/B$ after the linear background of each curve is subtracted, showing the Shubnikov–de Haas oscillations. (c) ρ_{xx} measured at 2 K and in a field along the $[02\bar{1}]$ direction. The red line represents a quadratic law. (d) The angular dependence of ρ_{xx} measured at 2 K and in 1 T. The red line is a best fit to $\cos^2\theta$.

The temperature dependence of the crossover field B_c is shown in Fig. 3(d). It defines the boundary between regime I and regime II depicted in Fig. 3(b). B_c is linearly proportional to temperature above $\sim$100 K. This strongly hints that the crossover is related to the competition between the thermal energy and a Zeeman type of energy, i.e., $k_B T/2$ vs $g^*\mu_B B_c$, where k_B is the Boltzmann constant, g^* is an effective g factor, and μ_B is the Bohr magneton. From the slope of the boundary we have $g^* \approx 40$, in good agreement with the g factor of this material [31].

We have also performed measurements in tilted magnetic fields. The measurement configuration is illustrated in the inset of Fig. 4(b). The LMR gradually vanishes when the magnetic field is tilted from the [100] direction to the $[02\bar{1}]$ direction, allowing a quadratic behavior to emerge. The ρ_{xx} data at $\theta = 90^\circ$ can be roughly fitted to a quadratic law below 6 T as shown in Fig. 4(c).

The tilting-angle dependence of ρ_{xx} was also studied by continuously rotating the sample in a field of 1 T at $T = 2$ K. Shown in Fig. 4(d) is the net ρ_{xx} subtracted from the originally measured data, based on the assumptions that $\rho_{xx}(90^\circ - \theta) = \rho_{xx}(90^\circ + \theta)$ and $\rho_{xy}(90^\circ - \theta) = -\rho_{xy}(90^\circ + \theta)$. The yielded $\rho_{xx}(\theta)$ can be fitted to the functional form of $\cos^2(\theta)$. We notice that similar magnetoresistance anisotropy was also observed by Liang *et al.* where the field was tilted from the [112] to the $[1\bar{1}0]$ direction with the current applied along the $[1\bar{1}0]$ direction [11].

To summarize our findings, positive and large LMRs up to 3100% in a field of 14 T were observed on Cd_3As_2 with a carrier density as low as 5.0×10^{16} cm^{-3}. This behavior occurs in the measurement configuration that the current is applied along the [012] direction and the magnetic field is applied along the [100] direction and when the temperature is low or the magnetic field is high such that the Zeeman splitting overwhelms the thermal smearing. When the magnetic field is tilted from the [100] direction to the $[02\bar{1}]$ direction, the LMR gradually fades away so that a quadratic law emerges.

To explain the LMR behavior, several mechanisms mainly in two types have been proposed previously. One believes that the LMR arises by picking up the Hall signal in an inhomogeneous sample [14,21]. In this picture, the sample is modeled as a network due to the existence of large mobility fluctuation. The low carrier density yields a large Hall signal on the network which eventually influences the ρ_{xx} measurement. This picture, first used by Parish and Littlewood [21] to explain the LMR in highly disordered $Ag_{2\pm\delta}Se$ and $Ag_{2\pm\delta}Te$, is not likely applicable to our samples which are high-quality single crystals.

In the other type of mechanism, the interpretation of the LMR relies on the formation of LLs. Abrikosov proposed that a linear quantum magnetoresistance arises when all electrons are filled into the first LL [18,19]. In this mechanism, the amplitude of the LMR depends on the carrier density but not on the mobility. These features seem to fit with our data, i.e., although the mobility changes roughly by a factor of 2 below $\sim$100 K, the carrier density remains almost constant [Fig. 2(d)] and so does the gross slope of the LMR [Fig. 3(a)]. However, the Abrikosov mechanism requires that all of the electrons are filled into the first LL, which is not true in our experiment. Figure 2(c) clearly shows that the LMR extends to very low magnetic fields where no SdH oscillation exists, i.e., no LL has been formed. And, Fig. 3(b) further shows that the formation of LLs in high magnetic fields and low temperatures just causes SdH oscillations superimposed on the LMR trend, being irrelevant to the LMR trend itself.

Magnetoresistance in ordinary metals is usually much smaller than the resistance itself. A LMR up to 3100% in a magnetic field of 14 T must be caused by some peculiar mechanisms in which the electron density of states or the scattering rate, or both, must be significantly modified by the magnetic field. Here the modification in the electron density of states would refer to the modification in the Fermi surface. And the modification in the scattering rate (hence the carrier mobility) would refer to the change in scattering processes which are likely prohibited originally in the zero magnetic field.

Among various possibilities, here we would draw attention to the field-induced relative shifting of the two Weyl-Fermi surfaces in momentum space. Cd_3As_2 contains two 3D Dirac cones in the first Brillouin zone in momentum space. Each Dirac cone further contains two Weyl-Fermi surfaces with opposite helicity. These two Weyl-Fermi surfaces, which are originally overlapping in the zero magnetic field, will be shifted apart in the momentum space upon the application of a magnetic field (illustrated in Fig. S6 of the Supplemental Material [27]). When the Fermi surfaces are small and very close to the Dirac points, such as the case in our samples, the shifting (proportional to $g^*\mu_B B$) becomes a dominant effect which could significantly influence the magnetotransport properties of the samples. From the data of the SdH oscillations shown in Figs. 3(b) and 4(b) in which the oscillation period remains almost unchanged over the entire $1/B$ range, we believe that the field-induced changes in the electron density of states are insufficient to account for the observed LMR up to 3100%. We therefore speculate that some scattering processes, which are otherwise protected in the zero magnetic field, might be released with the shifting of the Fermi surfaces in momentum space, giving rise to the LMR after the Zeeman splitting overwhelms the thermal smearing. We note that similar speculation on the lifting of protection to backscatterings has also been proposed by Liang and co-workers [11]. At the present stage, however, it is not clear to us why the shifting of Weyl-Fermi surfaces in momentum space could lift the protection.

Nevertheless, the above scenario could consistently explain why a large LMR is often observable in Dirac electron systems. Dirac electron systems possess all the key elements required for such a scenario, i.e., containing helical electrons, having small Fermi surfaces, yet with large Zeeman splitting due to large g factors. For Cd_3As_2 its $g^* \approx 40$, the Zeeman splitting is $\sim$23 meV at $B = 10$ T. This energy scale is comparable to the Fermi energy of $\sim$30 meV (Hall) or $\sim$52 meV (SdH) estimated from the carrier density of the sample [27].

To summarize, through analyzing the crossover behavior between the LMR and the quadratic one in Cd_3As_2, we revealed that the linearity of magnetoresistance occurs only when the amount of shifting of the Weyl-Fermi surface in momentum space overwhelms the thermal smearing. We hope that our finding this provides a useful clue for the final explanation of the LMR behavior.

Note added. After the first submission of this Rapid Communication and posted on the arXiv (arXiv:1405.6611), many groups have also reported the observation of large positive LMR on the Dirac semimetal type of materials [13,14] and Weyl semimetal type of materials [12,16,17].

We would like to thank C. L. Yang for helpful discussions. This work was supported by the National Basic Research Program of China from the MOST under Contracts No. 2009CB929101, No. 2011CB921702, and No. 2011CBA00110, by the NSFC under Contracts No. 91221203, No. 11174340, No. 11174357, and No. 11274367, and by the Knowledge Innovation Project and the Instrument Developing Project of CAS.

[1] M. N. Baibich, J. M. Broto, A. Fert, F. Nguyen Van Dau, F. Petroff, P. Etienne, G. Creuzet, A. Friederich, and J. Chazelas, Phys. Rev. Lett. **61**, 2472 (1988).
[2] A. P. Ramirez, J. Phys.: Condens. Matter **9**, 8171 (1997), and the references therein.
[3] R. Xu *et al.*, Nature (London) **390**, 57 (1997).
[4] F. Y. Yang *et al.*, Science **284**, 1335 (1999).
[5] J. Hu and T. F. Rosenbaum, Nature Mater. **7**, 697 (2008).
[6] A. L. Friedman *et al.*, Nano Lett. **10**, 3962 (2010).
[7] X. Wang, Y. Du, S. Dou, and C. Zhang, Phys. Rev. Lett. **108**, 266806 (2012).
[8] H. Tang *et al.*, ACS Nano **5**, 7510 (2011).
[9] J. Tian *et al.*, Sci. Rep. **4**, 4859 (2014).
[10] L. P. He, X. C. Hong, J. K. Dong, J. Pan, Z. Zhang, J. Zhang, and S. Y. Li, Phys. Rev. Lett. **113**, 246402 (2014).
[11] T. Liang, Q. Gibson, M. N. Ali *et al.*, Nature Mater. **14**, 280 (2015).
[12] C. Zhang, C. Guo, H. Lu, X. Zhang, Z. Yuan, Z. Lin, J. Wang, and S. Jia, Phys. Rev. B **92**, 041203(R) (2015).
[13] A. Narayanan, M. D. Watson, S. F. Blake *et al.*, Phys. Rev. Lett. **114**, 117201 (2015).
[14] M. Novak, S. Sasaki, K. Segawa, and Y. Ando, Phys. Rev. B **91**, 041203(R) (2015).
[15] S. Flynn, M. Ali, and R. J. Cava, arXiv:1506.07069.
[16] C. Zhang, Z. Yuan, S. Xu *et al.*, arXiv:1502.00251.
[17] X. Huang, L. Zhao, Y. Long *et al.*, arXiv:1503.01304.
[18] A. A. Abrikosov, Phys. Rev. B **58**, 2788 (1998).
[19] A. A. Abrikosov, Phys. Rev. B **61**, 7770 (2000).
[20] C. M. Wang and X. L. Lei, Phys. Rev. B **86**, 035442 (2012).
[21] M. M. Parish and P. B. Littlewood, Nature (London) **426**, 162 (2003).
[22] Z. Wang, H. Weng, Q. Wu, X. Dai, and Z. Fang, Phys. Rev. B **88**, 125427 (2013).
[23] M. Neupane *et al.*, Nat. Commun. **5**, 3786 (2014).
[24] Z. K. Liu *et al.*, Nature Mater. **13**, 667 (2014).
[25] S. Borisenko, Q. Gibson, D. Evtushinsky, V. Zabolotnyy, B. Büchner, and R. J. Cava, Phys. Rev. Lett. **113**, 027603 (2014).
[26] S. Jeon, B. B. Zhou, A. Gyenis *et al.*, Nature Mater. **13**, 851 (2014).
[27] See Supplemental Material at http://link.aps.org/supplemental/10.1103/PhysRevB.92.081306 for material synthesis, heat-capacity measurement, the estimations of carrier density, effective mass, the Dingle temperature from the data of the SdH oscillations, the theoretical analysis on the carrier density, Fermi energy, the Lifshitz transition, along with the illustration of the

shifting of two Weyl-Fermi surfaces in momentum space in the presence of an applied magnetic field.

[28] M. V. Stackelberg and R. Paulus, Z. Physik. Chem. B **28**, 427 (1935).

[29] G. A. Steigmann and J. Goodyear, Acta Crystallogr.. Sect. B: Struct. Crystallogr. Cryst. Chem. **B24**, 1062 (1968).

[30] M. N. Ali, Q. Gibson, S. Jeon, B. B. Zhou, A. Yazdani, and R. J. Cava, Inorg. Chem. **53**, 4062 (2014).

[31] H. E. A. Lamrani, M. J. Aubin, and L. G. Caron, J. Phys. C: Solid State Phys. **19**, 3151 (1986).